ACS NANO

www.acsnano.org

ARTICLE

Highly Ordered Boron Nitride/Epigraphene Epitaxial Films on Silicon Carbide by Lateral Epitaxial Deposition

James Gigliotti, Xin Li, Suresh Sundaram, Dogukan Deniz, Vladimir Prudkovskiy, Jean-Philippe Turmaud, Yiran Hu, Yue Hu, Frédéric Fossard, Jean-Sébastien Mérot, Annick Loiseau, Gilles Patriarche, Bokwon Yoon, Uzi Landman, Abdallah Ougazzaden,* Claire Berger,* and Walt A. de Heer

Cite This: *ACS Nano* 2020, 14, 12962–12971

Read Online

ACCESS | Metrics & More | Article Recommendations | Supporting Information

ABSTRACT: The realization of high-performance nanoelectronics requires control of materials at the nanoscale. Methods to produce high quality epitaxial graphene (EG) nanostructures on silicon carbide are known. The next step is to grow van der Waals semiconductors on top of EG nanostructures. Hexagonal boron nitride (h-BN) is a wide bandgap semiconductor with a honeycomb lattice structure that matches that of graphene, making it ideally suited for graphene-based nanoelectronics. Here, we describe the preparation and characterization of multilayer h-BN grown epitaxially on EG using a migration-enhanced metalorganic vapor phase epitaxy process. As a result of the lateral epitaxial deposition (LED) mechanism, the grown h-BN/EG heterostructures have highly ordered epitaxial interfaces, as desired in order to preserve the transport properties of pristine graphene. Atomic scale structural and energetic details of the observed row-by-row growth mechanism of the two-dimensional (2D) epitaxial h-BN film are analyzed through first-principles simulations, demonstrating one-dimensional nucleation-free-energy-barrierless growth. This industrially relevant LED process can be applied to a wide variety of van der Waals materials.

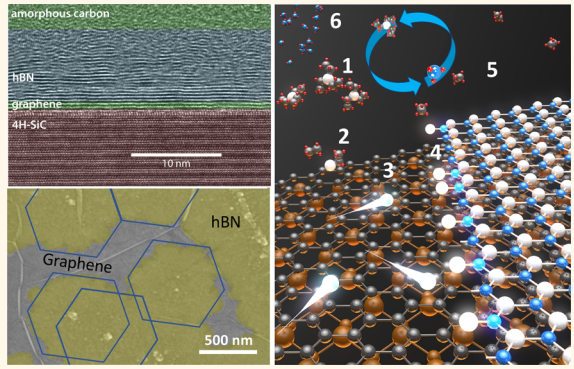

KEYWORDS: *graphene, boron nitride, silicon carbide, epitaxial growth, MOVPE, van der Waals heterostructures, ab initio calculations*

Van der Waals heterostructures have been proposed for many applications, of which high-performance electronics is the most challenging. Current methods to produce graphene/dielectric heterostructures typically result in contaminated or disordered interfaces. Since epitaxial heterostructures are necessary to enable graphene nanoelectronics, technologically viable production methods are essential.

Epitaxial graphene on silicon carbide (epigraphene or EG)[1] stands out, because the ultrahigh temperature vacuum growth process (>1500 °C) produces essentially defect-free graphene nanostructures that are crystallographically aligned with the single crystal hexagonal silicon carbide substrate. EG nanostructures have been produced with exceptional room temperature ballistic transport properties; ultrahigh-frequency transistors have been realized, and wafer-scale processing has been demonstrated (see ref 2 and references therein). That is why epigraphene qualifies as a leading two-dimensional (2D) technology platform for future high-performance nanoelectronics.

Further progress requires that van der Waals semiconductors or dielectrics can be directly grown on EG nanostructures, since all electronic devices require dielectrics for gating, tunneling junctions, and insulation. Common dielectrics, like Al_2O_3 and HfO_2, use atomic layer deposition (ALD) processes that require chemical modification or roughening of the graphene to facilitate adhesion. These processes cause a variety of problems (see ref 3 and references therein) like charged

Received: May 18, 2020
Accepted: September 23, 2020
Published: September 23, 2020

https://dx.doi.org/10.1021/acsnano.0c04164
ACS Nano 2020, 14, 12962–12971

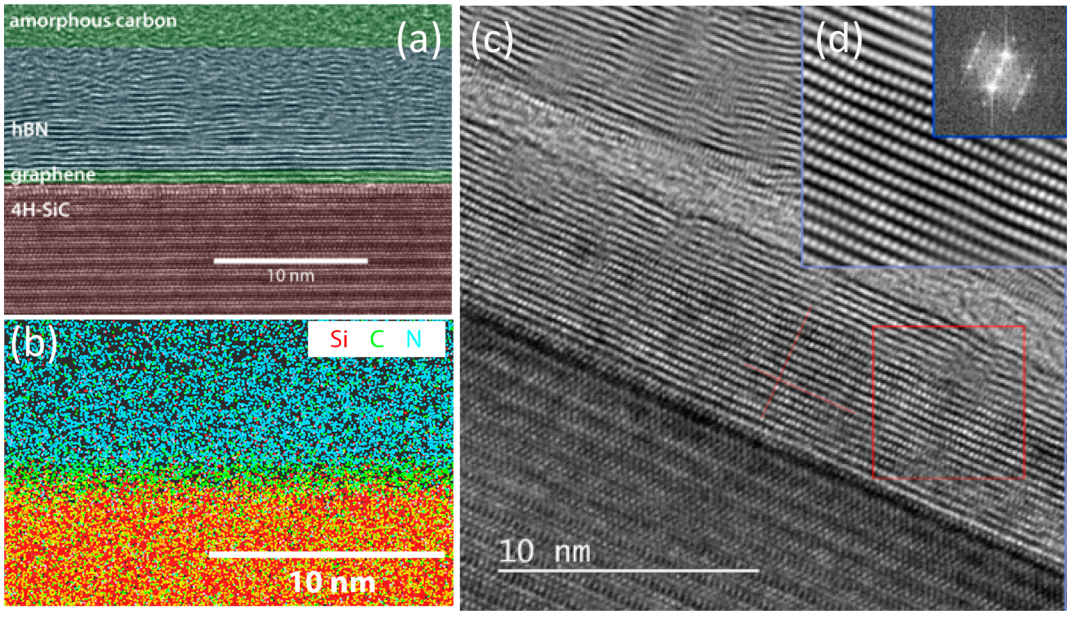

Figure 1. Cross-sectional HR-TEM of h-BN on epigraphene along the zone axis. (a) Colored high resolution image depicting coherence in the h-BN layer grown on one (possibly 2 layers) EG on the Si-face. Identification of the layers is obtained from the EDX analysis in (b). Disorder of the top h-BN layers is mainly due to Ga ion damage from the FIB preparation. The spacing of the first graphene layer is 0.43 nm, indicating hydrogen intercalation at the SiC/EG interface. (b) EDX analysis of the HR-TEM image in (a) chemically resolving the N atoms in the h-BN layer, the C atoms in the graphene layer, and the Si atoms in the SiC layer (sensitivity-limited detected B is shown in Figure S5 as well as FIB induced Ga contamination). (c) HR-TEM of another heterostructure, confirming that the h-BN layers are well ordered. (d) Zoom in the region in the red square in (c), showing an interlayer spacing of the h-BN layer of 0.345 nm and dominant AB stacking. Inset: fast Fourier transform showing AB stacking with some admixture of ABC stacking. (The disordered area between the well ordered layers is a separation between layers due to delamination during the thin slab preparation.)

surface states, surface roughness, impurities, and pinholes, which all compromise electronic performance.[3,4]

Here, we concentrate on hexagonal boron nitride (h-BN), a semiconductor with a bandgap over 6 eV and a dielectric constant of about 4. It is an isomorph of graphene, chemically inert, that can sustain extremely high temperatures. A lattice mismatch of only 1.7% makes it optimally compatible with epitaxial growth on graphene. Graphene deposited on h-BN or sandwiched between h-BN crystals shows much improved mobility.[5−10] However, these mechanical transfer processes are not scalable, and controlling the graphene−h-BN interface is problematic (trapped impurities, wrinkles, gas filled blisters).[11] Epitaxial h-BN growth has been demonstrated on metal substrates up to wafer scale,[12−15] but this process requires transfer onto graphene, resulting in contaminated and otherwise defective interfaces. Since electronic transport in graphene is sensitive to the alignment with h-BN,[16−18] a perfect lattice alignment of the h-BN and graphene is required for reproducible nanoscale electronics applications; therefore, transferred materials cannot be used. Early attempts[19−26] to grow h-BN on graphene by conventional chemical phase deposition (CVD) methods or by molecular beam epitaxy[26] were met with limited success in terms of grain size, coverage, and graphene integrity or were left with open questions concerning the interface quality and integrity of the graphene layers. Conventional growth of van der Waals semiconductors (MoS_2,[20,27,28] WS_2,[29] WSe_2,[20,30,31]) as well as h-BN[19−25] on graphene often deteriorates from individual single-layer platelets to regions of inhomogeneous thickness as growth proceeds and, even more seriously, results in poor interfaces and even B/N substitution with carbon of the graphene.

Recently, migration-enhanced metalorganic vapor phase epitaxy (ME-MOVPE) has been used to grow h-BN on silicon[32] and sapphire[33−35] substrates. In this high temperature process, triethylboron (TEB) and ammonia (NH_3) are used to produce a multilayer h-BN film on the sapphire wafer, informing the present approach.[33] We present here direct evidence that the ME-MOVPE process yields atomically sharp h-BN/graphene epitaxial interfaces, with a templated h-BN growth on graphene. This result, combined with the industrial compatibility and fast growth process, makes MOVPE a method of choice.

Conventional atomic layer deposition is a cyclic process involving two different precursor molecules in the gas phase that are alternately introduced on a surface and in which each cycle deposits exactly one atomic layer on top of the film. In contrast, in the migration-enhanced lateral epitaxial deposition (LED) mechanism that we propose here, each cycle "knits" one row of atoms to the edge of the growing multilayer film. The process presented here demonstrates that the method produces high quality BN−graphene interfaces and provides a clear path toward further improvement.

RESULTS AND DISCUSSION

The LED process proceeds in a MOVPE growth chamber in which the TEB and NH_3 volatile molecules that are the precursors for the h-BN films are introduced to the extremely hot EG on the SiC wafer. Contrary to most CVD processes used to grow h-BN, the key steps here are the sequential introduction of the chemicals and the rest time between the two injections. A growth cycle consists of first a pulsed injection of TEB that is transported in a flow of hydrogen carrier gas, followed by a purge and then by a similar sequence

https://dx.doi.org/10.1021/acsnano.0c04164
ACS Nano 2020, 14, 12962−12971

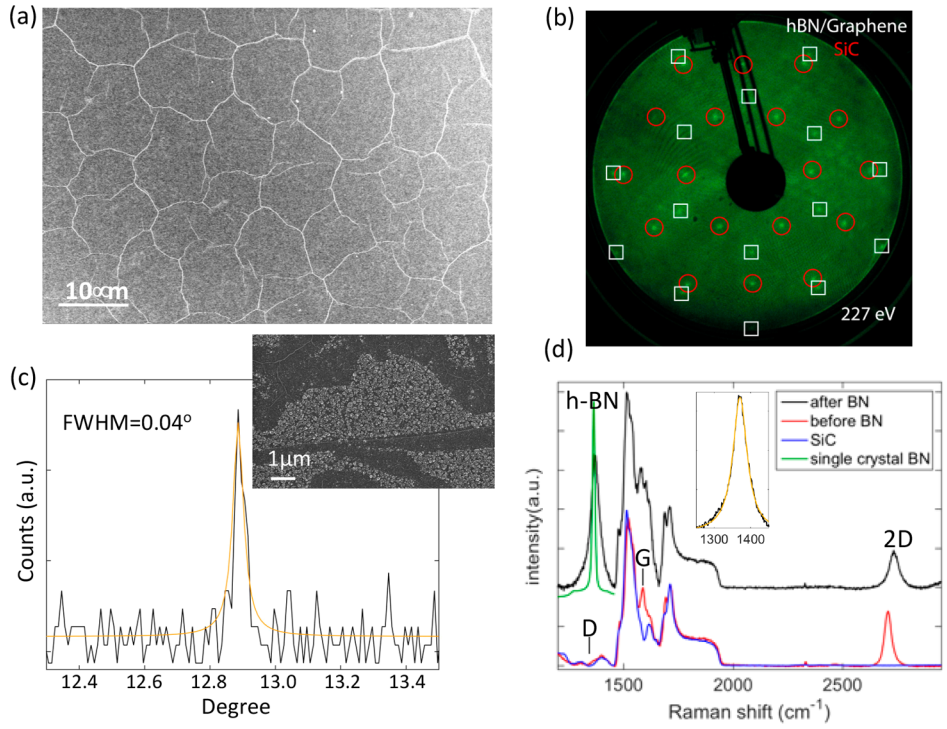

Figure 2. Analysis of an h-BN/EG/SiC heterostructure. (a) SEM image of an h-BN film prepared on a monolayer epigraphene of the Si-face (SiC(0001)), showing a homogeneous full coverage. White lines are pleats. (b) Low energy electron diffraction performed with a 227 eV electron beam, showing the expected h-BN, EG, and SiC diffraction spots. The relative azimuthal orientation of the spots and the absence of rings and other anomalies confirm the epitaxy of the heterostructure h-BN/EG/SiC. (c) The HR-XRD rocking curve has a full width at half maximum (fwhm) of 0.04°, demonstrating the extreme flatness of the film layers. Inset: SEM image of h-BN coating on a partially graphitized SiC surface, composed of EG ribbons (grown on natural SiC substrate step walls) separated by buffer layer regions, showing the smooth h-BN/EG surface (dark areas), compared with the rough h-BN/buffer layer surface caused by the very high density of nucleation sites on the buffer layer. (d) Raman spectra of a few graphene layers on the carbon face (red) compared to the bare SiC spectrum (blue). The Raman spectrum after h-BN growth (black) displays a large peak at 1370 cm^{-1} that is ascribed to the h-BN E_{2g} due to the absence of a D peak in the as-grown EG. (For this spectrum, the disordered top h-BN layers are mechanically removed.) Inset: Lorentizan fit of the peak at 1370 cm^{-1} (fwhm = 47.3 cm^{-1}).

for the injection of NH_3 (see Methods for details and ref 33). In this process, the TEB and NH_3 precursors alternatively decompose on the hot EG surface, thereby providing active boron and then nitrogen atoms to form the h-BN layers.

In the following, we present properties of the h-BN films grown on EG on the (0001) Si-face and the (000$\bar{1}$) C-face of 4H-SiC and on natural EG nanostructures on both the Si- and C-faces. We demonstrate that the h-BN films consists of 2D sp^2 layers and that the first h-BN layers are in epitaxy with epigraphene. Figure 1a−d shows cross-sectional, high-resolution transmission electron microscopy (HR-TEM) images of the h-BN/EG/SiC heterostructures, composed of h-BN on monolayer EG on the Si-terminated face (Figure 1a,b) and h-BN on a few EG layers on the C-terminated face of hexagonal SiC (Figure 1c,d). At the interface in particular, the h-BN layers are atomically flat and very well ordered. Close examination of the HR-TEM image of Figure 1d shows AB stacking of the h-BN layers. Fast Fourier transform (FFT) analysis confirms this stacking (Figure 1d, inset) and also reveals some admixture of ABC stacking[36] (see also Figures S2 and S3).

This stacking order continues throughout the film and particularly at the critically important h-BN/EG interface (Figures 1, S2, and S3). This is consistent with the epitaxy of the h-BN film on the graphene (see below). Extended disordered grain boundaries or discontinuities were not observed at the h-BN/graphene interface in any of the twelve 70 nm sections of cross sectional HR-TEM images spanning the 1.5 μm size thin slab that was examined in detail. This suggests that, during growth, h-BN sheets lock in place, rather than simply lay on top of the graphene. The local misorientation observed in the uppermost layers in thick h-BN films (Figure 1a,b) is largely caused by the HR-TEM slab preparation using a focused gallium ion beam, as evidenced by the presence of Ga in those films (see Figure S5), due to an insufficient protection by the deposited carbon layer.

Energy dispersive X-ray spectroscopy (EDX) in Figure 1b identifies chemical components at various depths in the film and correlates with the chemical assignments in Figure 1a (see Figure S5 for further analysis). The graphene layers are clearly identified, and uniform composition of the h-BN layers is shown.

These results are confirmed by electron energy loss spectroscopy (EELS); see Figure S6. In particular, the B spectra in the film presents a narrow and intense sharp π^* peak at 191.1 eV, which is a defining characteristic of sp^2-hybridized B atoms. Composition analysis with X-ray photoemission spectroscopy (XPS) has the same line profile as a reference h-BN single crystal (see Figure S7) and gives the same B/N ratio; the flatness of the h-BN layers also indicates a 1/1 boron to nitrogen stoichiometric ratio. XPS profile analysis further indicates a carbon composition of at most about 3% in the h-

https://dx.doi.org/10.1021/acsnano.0c04164
ACS Nano 2020, 14, 12962−12971

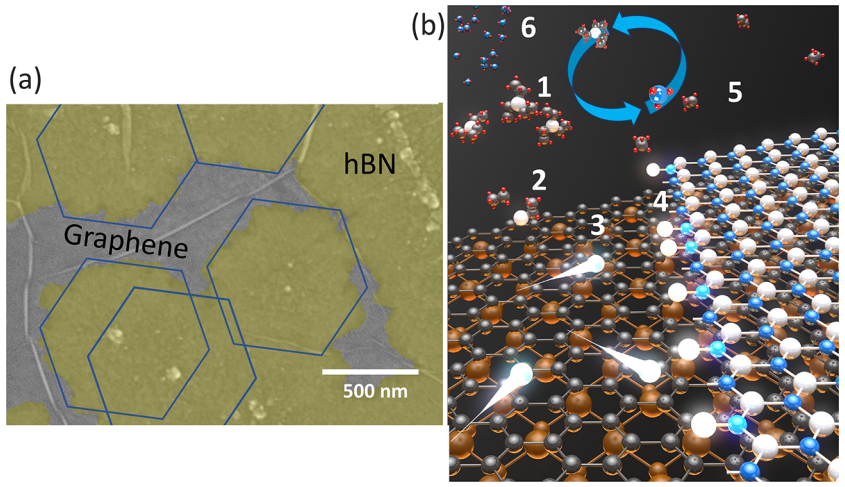

Figure 3. (a) Colored SEM image showing a partially grown multilayer h-BN film on a multilayer C-face graphene after 1200 LED cycles. The size of the hexagonal 2D h-BN crystallites corresponds with the expected size for roughly one atomic front growth per cycle. The hexagons merge (they do not overlap), ultimately producing a single continuous sheet (see text). The large pleats on the bare graphene areas are commonly seen for the graphene on the C-face. (b) Schematic of the formation of the epitaxial 2D heterostructure using the lateral ALD process. The process cyclically injects TEB and then ammonia. In the depicted TEB phase of the cycle, TEB (1) decomposes on the hot epigraphene surface liberating ethane (2) that escapes. The free, highly mobile boron atom (3) skids on the epigraphene to an awaiting nitrogen atom at the edge of the growing film (4). The process terminates when all nitrogen sites are passivated and is ready for the second half of the cycle where the remaining TEB and ethane are purged (5) and ammonia is introduced (6) to add a fresh row of nitrogen to the boron saturated edge by the analogous decomposition process.

BN film. This carbon content was determined after etching the spurious surface carbon of h-BN deposited on a sapphire substrate placed next to the EG/SiC substrates during the deposition runs. All the other XPS peaks are similar between h-BN on both substrates, and there is no contribution from sp^2 carbon.

The h-BN layer spacing, observed by HR-TEM in Figure 1a,c as 0.345 nm, is very close to the bulk h-BN (0.333 nm), which is consistent with multilayer h-BN on sapphire.[37] On the Si-face EG, the first graphene layer is located 0.43 nm above the topmost SiC, in agreement with the spacing reported for quasi-freestanding epigraphene following hydrogen passivation of the SiC surface[38] and lifting up of the buffer layer. Hydrogen intercalation is consistent with the XPS C 1s spectra where the characteristic component of the buffer layer is not observed (Figure S7). It also agrees with LEED observations (Figure 2b, see below) and with the preliminary measurement of a large density of positive charge carriers ($\approx 10^{13}$ cm^{-2}) for the Si-face EG under h-BN. This indicates that a quasi-freestanding bilayer graphene is easily produced by the LED method. When helium, instead of hydrogen, is used as the carrier gas, this conversion of the buffer layer to freestanding graphene is expected to not occur, thereby conserving the pristine monolayer graphene on top of the buffer layer.

Figure 2 compiles significant characterization results that are discussed next. (See the Supporting Information for details.) The scanning electron microscopy (SEM) image of Figure 2a, taken for a 45 nm thick h-BN film grown on Si-face EG, shows a continuous and homogeneous film with a network of 3-fold connected pleats. The quasi-hexagonal pleat pattern (see also Figure S9d) is indicative of an isotropic uniform contraction of 2D layers upon cooling (similar to multilayer C-face EG layers[2]), with no sign of pinning, tearing, or large defects. Note that the EG monolayer onto which the h-BN is grown has no pleats, as is common for EG on the Si-face (see Figure S1a). Low energy electron diffraction (LEED) in Figure 2b shows the diffraction pattern of the h-BN/EG/SiC heterostructure. The diffraction pattern was recorded with a relatively large electron energy (227 eV) to penetrate through the h-BN and graphene layers and into the SiC, thereby producing a composite diffraction image. The h-BN diffraction spots are registered with the graphene spots; both are rotated 30° with respect to the SiC. No rings or supplementary spots are observed, which would result if the h-BN layers were rotationally disordered. This observation is consistent with the epitaxy of all three components of the h-BN/EG/SiC heterostructure. The absence of satellites around the graphene spots is consistent with buffer layer lift up by hydrogen intercalation.[39]

High resolution X-ray diffraction (HR-XRD) that quantifies the atomic layer spacing was performed before and after the h-BN deposition on both the C-face and Si-face EG. The h-BN layer spacing was found to be 0.35 nm (Figure S4), consistent with the HR-TEM (Figure 1d). The rocking curve measurement of the h-BN (0002) peak (Figure 2c) gives an extremely narrow full width at half-maximum of 0.04°, which attests to the h-BN film high degree of parallel order that extends over the width of the X-ray beam (several mm^2, which is about the size of the sample).

Raman spectroscopy (Figure 2d) was performed before and after h-BN deposition. An example is given in Figure 2d for a few-layer C-face EG. Before h-BN coating, the absence of a Raman D-peak at 1350 cm^{-1} attests to the high quality of the multilayer EG (red trace to be compared with the SiC Raman peaks, blue trace). A large peak develops after h-BN coating at the expected energy of the h-BN E_{2g} peak (1370 cm^{-1}). The peak is prominent on areas where the top (disordered) h-BN layers were mechanically removed, attesting to the quality of the h-BN layers closer to the SiC interface. The effect of h-BN deposition on the graphene quality was further investigated by exfoliating the h-BN layer to expose the underlying graphene layer. The Raman spectra show no significant D peak after

https://dx.doi.org/10.1021/acsnano.0c04164
ACS Nano 2020, 14, 12962−12971

deposition, indicating that the graphene layer was not damaged in the process (see Figure S12), in agreement with the excellent h-BN/EG interface quality observed in HR-TEM.

The h-BN deposition was repeated on EG samples that were deliberately grown with incomplete graphene layers to produce EG nanoribbon-like structures on both Si- and C-faces, without resorting to lithographic patterning (Figures 2c, inset and S9b,c). After processing, the EG structures are covered with a high-quality uniform h-BN layer, while the remaining buffer layer areas are covered with poorly ordered h-BN crumpled sheets. These observations are consistent with the smooth, homogeneous, and defect-free EG nanostructures with h-BN nucleation at the edges. In contrast, the buffer layer has an excess of nucleation sites (due to its inherent 6 × 6 corrugations) that result in the rough h-BN structure. Note that for graphene nanoelectronics a high degree of h-BN order is required only on the EG nanostructures themselves. The growth of smooth layered BN on top of EG is in stark contrast with the preferential h-BN growth on the metallic substrates instead, promoted by the graphene edges in CVD processes (see for instance refs 40 and 41).

The h-BN dielectric quality was tested in a simple 2-probe transport measurement by measuring the $I-V$ characteristic from graphene to a top-gate evaporated on h-BN/EG. The area of the 1 μm^2 gate is largely compatible with the size of nanoelectronics devices, providing a good indication of the h-BN property in a functional device. The resistance of the h-BN film, measured perpendicularly to the stack, is of the order of 8 GΩ, and breakdown was observed above 165 V (see Figure S8), which is sufficient to raise the charge density on the EG to about 5 × 10^{13} cm^{-2}, *i.e.* an order of a magnitude more than required for intended electronic applications. Nevertheless, larger values are expected with higher quality films. The tested nine top gates gave similar results, showing excellent homogeneity of the dielectric properties, despite the presence of h-BN pleats under some of them (see Figure S8).

Turning to the growth process, Figure 3a shows a scanning electron microscope image of the growth on C-face EG after 1200 cycles, showing several merging, quasi-hexagonal h-BN crystallites that nucleated at several random points on the graphene surface. The parallel orientation of the hexagons indicates epitaxy. The size of these crystallites correlates with the number of cycles; in this case, each cycle adds on average about one and a half BN rows to the crystallite per cycle.

Growth dynamics on the surface of the EG can therefore be understood in the following way, as depicted in Figure 3b. At the hot graphene surface where the TEB molecule decomposes after the TEB pulse injection, the liberated highly mobile boron atom migrates over the graphene surface and attaches to the thermodynamically favorable nitrogen terminated edge of the h-BN film (see theoretical simulation below). To avoid Volmer−Weber 3D growth mode, excess boron atoms have to desorb, which is enabled by the growth-stop step where the chemical residuals (B and methyl compounds) are purged. A NH_3 pulse injection follows. The NH_3 decomposes on the surface to produce a nitrogen atom that attaches to the boron atom at the edge of the nascent h-BN film. The carrier gas desorbs other volatile decomposition products. In this way, (ideally) a single row of h-BN is added to the edge of the growing film in each cycle of the LED process. This process also applies to subsequent h-BN layer growth, mediated by the fast B and N atom diffusion on the h-BN surface, similar to the graphene surface.

We emphasize that the lateral growth process described above is not limited to monolayers but applies to multilayers as well, giving rise to the uniform multilayers observed in Figure 3a. The process can be understood as follows. Once initiated at a nucleation site, a multilayer growth front will propagate laterally, where B and N atoms alternatively attach to the vertical front. B and N atom diffusion is mediated as described above, on both on the uncoated graphene and on the growing multilayer h-BN crystal. Hence, the thickness of the film is defined by the properties of the nucleation site, as is typical in crystal growth in general. For clean graphene, h-BN nucleation is initiated at the graphene edges and the lithography used to define the graphene nanostructures will need to be optimized to control the BN film thickness.

More systematic studies of different growth conditions and growth rates for fine-tuning of the processes will follow in further experiments, in particular by iteratively adjusting the boron precursor flow rate. Systematic optimization for specific applications is routine in all deposition processes. The optimization of the many parameters can be efficiently guided by simulations that provide insight into the processes, as demonstrated below. In particular, the observed hexagonal grains with dendritic edges (Figure 3a) result from diffusion limited growth conditions, as expected for ordered growth without a free-energy barrier or critical nucleus size, as demonstrated and elaborated by the numerical simulation below. For van der Waals material growth in general, grains can vary in shape from triangular to a truncated triangle to hexagonal, depending on the specific growth kinematics, temperature conditions, and substrates.[42,43] In the process presented here, the B and N precursors are introduced in the growth chamber, separated with a purge. These growth conditions with optimized precursor ratios ultimately allowed the achievement of hexagonal grains with uniform stoichiometry. In addition, the next generation of ME-MOVPE will involve higher temperatures, since an increase in the temperature is known to promote a straight growth front. This is also expected to inhibit the nucleation of subsequent layers and provide a better control of the film thickness.

To explore the structural evolution and energetics of the atomic-scale mechanisms underlying the h-BN film growth processes, we performed first-principles density-functional theory (DFT) simulations; for details, see the Methods and Supporting Information. To this end, we modeled the graphene surface by a periodically replicated supercell (6 × 12 hexagons comprising 144 C atoms, with an energy optimized interatomic distance (d_{C-C}) of 1.425 Å) on which we adsorbed a partial strip of h-BN; see the configuration of h-BN/graphene in Figure 4a. Such an initial configuration could be formed by considering a graphene sheet exposing a free edge, serving to initiate the alternating adsorption of B and N rows (following the fast diffusion of the atomic constituents on the bare graphene surface). Our simulations illustrate the atomic-scale mechanisms governing such a row-by-row growth process.

To simulate the growth of the h-BN film, we focus on two growth modes: (I) where, subsequent to thermal decomposition of the incident (alternating) TEB and NH_3 precursors on the graphene with a heated surface T > 1500 K, we consider low fluxes (LF) of B (boron) and N (nitrogen) atoms arriving (through low-barrier thermal diffusion (see the Supporting Information) on the bare graphene surface) to the vicinity of the h-BN growth front, and (II) where for each of the growth

https://dx.doi.org/10.1021/acsnano.0c04164
ACS Nano 2020, 14, 12962−12971

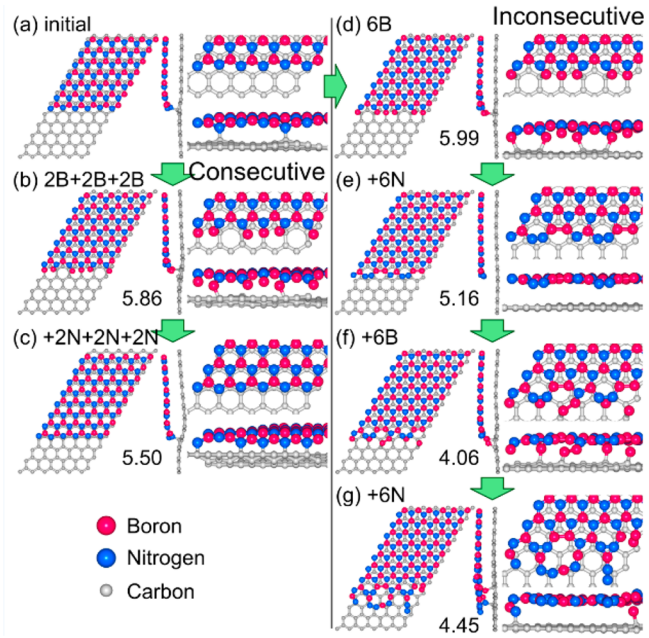

Figure 4. First-principles calculated mechanism of the growth of an h-BN film on epigraphene. The DFT model system consists of a graphene surface composed of 6 × 12 hexagons, periodically replicated in the *xy* plane, partially covered by an h-BN strip. Boron atoms are depicted as red balls; nitrogen atoms are blue, and carbon atoms are gray. In each of the panels (except for panel a), we include the DFT-calculated binding energy (per B or N atom) in eV units, associated with the corresponding stage of h-BN film growth shown. (a) The energy optimal initial configuration, showing a partially grown h-BN film adsorbed on the graphene surface. A top view is shown on the left. In the middle, we show a side view illustrating the "floating" nature of the partially grown h-BN film. At the top right, a zoomed view (from above) of the edge of the h-BN film is depicted, showing nitrogen termination of the growing front, with two of the N atoms bonded to the graphene surface. Below the above view, we show an enlarged view taken normal to the growing film edge, illustrating the weak coupling between the h-BN film and the graphene substrate. In (b), we depict the optimal configurations, resulting from exposure of the initial configuration (in a) to a low flux (LF) of B atoms. The small flux is modeled via the consecutive adsorption of boron atoms (2B atoms at each adsorption stage), with the system allowed to relax to the energy-optimal configuration after each adsorption step (for a detailed view of the system after each of the three consecutive B-adsorption steps, see Figure S15). The configuration shown in (b) is the one obtained at the end of the consecutive adsorption 2B + 2B + 2B process (resulting in 6 adsorbed B atoms corresponding to the 6 edge-exposed N atoms). Note that in this configuration all the adsorbed B atoms are bonded to both the nearest edge-N atoms of the film as well as anchored (to various degrees) to the underlying graphene surface. (c) The consecutive adsorption of nitrogen atoms (low flux) results in the formation of an added row of perfect h-BN to the growing film. Five out of six of the N atoms at the bottom edge of the freshly grown hexagon row are anchored to the graphene surface. (d–g) An inconsecutive growth process, corresponding to high flux, HF, of arriving boron atoms followed by HF of impinging nitrogen atoms; that is, in each B/N cycle, all the boron as well as all the subsequent nitrogen atoms arrive (essentially) simultaneously to the growing edge of the h-BN film (with no, or incomplete at best, intervening structural relaxations taking place at the growth front; see initial configuration in (a) followed by the configurations in (d)), resulting in defective growth of the film (see configuration in (e)). The subsequent HF adsorption cycle yields a disordered film edge (see (g)).

cycles we consider (alternating) high-fluxes (HF) of B and N atoms impinge on the h-BN film growth front. For our model system, each growth cycle entails impingement of 6 B atoms followed by 6 N atoms, resulting, under optimal growth conditions, in the formation of 6 new h-BN hexagons after each cycle. In simulations of the LF mode, we divide (in each cycle) the approach of the 6 B atoms into three stages (two B atoms in each stage, 2B + 2B + 2B), with the system allowed to structurally and energetically relax to the lowest energy configuration after each stage of 2B atom diffusion-and-attachment to the film edge. A similar consecutive impingement-followed-by-relaxation procedure is used for the subsequent 6 N (2N + 2N + 2N) atoms, completing the growth cycle.

LF growth, resulting in perfect hexagonal order at the additional freshly grown h-BN film edge, is shown in the a–b–c sequence in Figure 4. Note the bonding to graphene of the N atom at the growth edge of the h-BN film and the debonding (compare Figure 4b,c) of the edge B atoms induced by the impingement of the N atoms, which bond to the film-edge B atoms; a detailed view of the LF growth mechanism and the corresponding structural parameters are given in Figure S15. The binding energies, per B atom (5.86 eV) and per N atom (5.50 eV), at the end of the B and N parts of the cycle, respectively, are noted in Figure 4b,c; these binding energies are obtained from the calculated total energy differences corresponding to the system before and after the diffusion and attachment of the graphene-surface-adsorbed B and N atoms to the growth front of the h-BN film (see the Supporting Information for details). The binding energy per BN unit in the freshly grown h-BN front row is E_b(BN) = 5.86 + 5.50 = 11.36 eV. Subsequent LF cycles yield a perfectly ordered h-BN film. Interestingly, bondings of B and N atoms to graphene are found to occur only at the edge (growth front) of the h-BN film (see Figure 4), whereas away from that edge, only weak interaction is found between the h-BN film and the underlying graphene surface (DFT calculated to be 0.13 eV per BN unit). Furthermore, as observed from the comparison of the edge configurations in Figure 4a,b, the attachment of B atoms debonds the edge N atoms from the graphene surface. In turn, we find now graphene-surface-bonded B atoms (Figure 4b); these atoms debond in the course of the subsequent attachment of N atom as the B and N deposition cycle completes (Figure 4c). Such bonding–debonding processes at the growth-edge repeat and accompany, throughout, the growth process of the (essentially) perfectly ordered h-BN film. The geometrical parameters corresponding to each of the panels (a–g) are given after Figure S14.

It is instructive to contrast the above LF results with those obtained from a simulation of the HF growth mode, also termed "inconsecutive" process. Starting from the same initial state, we observe at the end of the first (6B + 6N) cycle (see Figure 4a,d,e) a disordered film edge (with a calculated E_b(BN) = 11.15 eV). The subsequent cycle (Figure 4f,g) results in a highly disordered state, with a significantly decreased binding E_b(BN) of 8.51 eV. The superiority of the low-flux (consecutive) growth mode is evident, owing to the structural relaxation/annealing, enabled by the lower rate of impingement of the film's atomic constituents.

We conclude by commenting on the 1D row-by-row growth model[44] of the epitaxial h-BN film, illustrated by our LF simulation. Our simulations uncover ordered growth without a free-energy barrier or critical nucleus size. Indeed, such a

https://dx.doi.org/10.1021/acsnano.0c04164
ACS Nano 2020, 14, 12962–12971

growth "anomaly" has been long-predicted by classical nucleation theory (CNT)[44,45] (attributed to J. Williard Gibbs), since in 1D both contributions to the free-energy-change upon phase change [the first contribution associated with a *decrease* of the chemical potential caused by the formation of a nucleus of the new phase (*e.g.*, growth of a crystalline film) and the second one describing the *increase* in energy due to the interface formed between the nucleus and its surrounding] scale linearly with the length of the nucleus (unlike the case in 2D and 3D growth modes); thus, in 1D, there is no length-scale interplay between the two contributions to the free-energy, and consequently, no nucleation barrier or a critical-nucleus size apply here. The above does not preclude the involvement of other activation barriers (kinetic in nature), including a barrier for dissociative adsorption of the B and N precursor molecules, diffusional barriers of the B and N atoms, or chemical attachment barriers. However, the h-BN film growth described in this work appears to not be hampered by such barriers, resulting in an effective growth of a highly ordered h-BN film on graphene.

CONCLUSIONS

In summary, a potentially industrially scalable MOVPE-based lateral epitaxial deposition process has been developed to produce high quality h-BN epitaxial films on EG. The crystalline quality and uniformity of the films and the clean epitaxial h-BN/EG interface were verified using a comprehensive suite of surface probes (SEM, HR-TEM, HR-XRD, XPS, EDX, EELS, LEED, and Raman spectroscopy). For a short growth time, incomplete coverage reveals that the first h-BN layers have large grains that are rotationally aligned to the SiC substrate. First-principles DFT simulations have uncovered a 1D nucleation-free-energy-barrierless growth mechanism of the epitaxial h-BN film. Atomic-scale details of the row-by-row growth are calculated, illustrating the role of atomic-scale relaxation processes at the 2D film growth front, in correlation with the perfection of structural ordering of the grown h-BN film that indicates the needed control over the fluxes of the constituents (B and N) in the LED process.

The observed uniform thickness and high crystalline quality over a large area offer the potential for improved reliability and performance in graphene-based nanoelectronics compared to traditional LED methods. Furthermore, since the extent of the prepatterned EG devices is typically less than 100 nm in nanoelectronics, the device edges are ideally suited as nucleation sites to initiate the line-by-line knitting film growth, which can be completed in less than 1000 cycles. In an optimized LED process, the cycle time can be optimized further. The h-BN/epigraphene/SiC heterostructure produced here presents the added advantage of being grown on a commercial single crystal semiconductor in an industrial reactor with 3 × 2 in. wafer capability. Moreover, the processes can be further expanded by growing an epitaxial graphene layer on top of the BN layers, using CVD.[46] In this way, graphene/h-BN/graphene heterostructures can be produced. This lateral LED process represents an important enabling step toward the realization of epigraphene nanoelectronics. The technique can be readily adapted to other van der Waals materials, such as MoS_2, to enable multilayer van der Waals epitaxial heterostructures of them as well.

METHODS

Epigraphene was produced on commercial chemical mechanical polished (CMP) insulating 4H-SiC substrates (from CREE). Complete few-layer graphene films as well as incomplete monolayer graphene domains separated by buffer layer areas were grown on the silicon terminated face (SiC-(0001)), as shown in Figure S1. Monolayer and multilayer epigraphene domains were produced on the carbon terminated face (SiC-$(000\bar{1})$) (Figure S1). The confinement controlled sublimation growth method was used, as described elsewhere,[47] to ensure graphene uniformity across the SiC surface. For this, the vacuum induction furnace was pumped down to 5×10^{-7} mbar prior to growth. SiC dies were outgassed at 800 °C prior to ramping to growth temperatures between 1400 and 1600 °C for 10−30 min, depending on the desired morphology. Incomplete graphene layers were also grown on 4H-SiC natural steps separated by large atomically flat terraces (5−20 μm).[48] For comparison, bare CMP 4H-SiC chips were also processed together with the graphene samples in the same MOVPE deposition runs. The above-mentioned graphene morphologies (single and multilayers, partially grown layers, and nanostructures) were used for h-BN film growth.

A migration-enhanced metalorganic vapor phase deposition process was applied for h-BN growth using an Aixtron close coupled showerhead 3 × 2 in. MOVPE reactor. Prior to growth, the chamber was heated to 1270 °C in a hydrogen environment at 85 mbar. A triethylboron (TEB) preflow (5−10 s) preceded the alternate introduction of TEB and ammonia (NH_3) to nucleate and grow the h-BN layers. A cycle consists of first a pulsed injection of TEB (1−3 s), where the total carrier gas flow rate was maintained at 20 SLPM with a TEB flow rate of 60 μmol/min. This is followed by a 1−3 s purge of the volatile components. Then, NH_3 is introduced for 3−6 s (flow rate: 1.35 SLPM; carrier gas: 20 SLPM), followed by a 1−3 s purge similar to a standard ALD process. The cycle is repeated for full coverage. h-BN films were grown with thicknesses ranging from about 1 to 50 nm. The growth rate in the *c*-axis direction was 5 nm/h as determined by AFM (scratch profile). The growth rate on EG was about 1/3 of that observed on sapphire (15 nm/h),[33] likely due to a lower nucleation density on the graphene surface migration-enhanced MOVPE process being applied to reduce excess nucleation on the surface of growing BN layers. Experience from BAlN and BGaN nitride MOVPE deposition studies indicates that the simultaneous introduction of precursors leads to lower nitride quality achieved than that achieved with the alternative protocol.[49]

For the cross-sectional HR-TEM study, 70−80 nm thick lamellae were prepared by FIB milling, following deposition of 50 nm of amorphous carbon (Figures 1a,b, S2, S5, and S6) or Pt (Figures 1c,d and S3) to protect the h-BN and graphene from ion bombardment and to reduce delamination. The images were taken along the $[11\bar{2}0]$ zone axis on a Titan Themis microscope at 200 kV. EDX was performed to determine the extent of Ga-ion damage, differentiate graphene and h-BN, and examine the chemical uniformity of the film.

The first-principles electronic structure calculations were performed with the Vienna *Ab initio* Simulation Package (VASP). A plane-wave basis with a kinetic energy cutoff of 400 eV and a *projector augmented wave (PAW)* pseudopotentials method[50] with the PBE generalized gradient approximation (GGA) for the exchange−correlation potential and including van der Waals interactions were used.[51] We employed a lattice parameter of 2.468 Å (C−C bond length of 1.425 Å) for the two-dimensional unit cell of a graphene's hexagonal lattice; these values were found from our DFT energy optimization (minimization) calculations. A unit cell of the graphene lattice contains two carbon atoms. We employed a graphene calculational unit cell composed of 6 × 6 hexagons (72 C atoms) for the boron and nitrogen atom adsorption calculations (see the Supporting Information) and a 6 × 12 (144 C atoms) graphene calculational cell for the h-BN film-growth simulations; the calculational cell was repeated periodically. An initial h-BN strip of 6 × 6 hexagons was constructed from 42 boron and 42 nitrogen atoms with the same lattice parameter as graphene, and it was positioned on the 6 × 12 graphene surface and subsequently energy optimized; the initial

https://dx.doi.org/10.1021/acsnano.0c04164
ACS Nano 2020, 14, 12962−12971

BN strip (see Figure 4a) comprised 912 valence electrons. Most of our calculations were performed using a single k-point sampling (that is Γ-point calculations); we checked that the results of h-BN growth remained essentially the same by employing (3 × 3 × 1) and (6 × 6 × 1) sampling of the surface Brillouin zone (see the Supporting Information).

In the simulation of the h-BN film growth process, for both the low-flux (consecutive) and high-flux (inconsecutive) modes, the adsorbed B or N atoms were initially located (adsorbed) on the bare graphene surface at a distance of up to 5 Å from any atom of the h-BN film growth front to ensure no direct initial bonding to the film. The attachment of the atoms to the film-growth front occurred in the course of (unconstrained) DFT energy minimization of the total system.

ASSOCIATED CONTENT

Supporting Information

The Supporting Information is available free of charge at https://pubs.acs.org/doi/10.1021/acsnano.0c04164.

Additional data on (1) epigraphene morphology, (2) h-BN crystal structure, (3) h-BN chemical and dielectric characterization, (4) h-BN surface morphology, (5) epigraphene characterization, and (6) theory (PDF)

AUTHOR INFORMATION

Corresponding Authors

Claire Berger − *Institut Néel, CNRS-Université Grenoble Alpes, 38042 Cedex 9 Grenoble, France; School of Physics, Georgia Institute of Technology, Atlanta, Georgia 30332, United States; Unité Mixte Internationale 2958, CNRS-Georgia Tech, 57070 Metz, France;* orcid.org/0000-0001-8341-2331; Email: claire.berger@cnrs.fr, claire.berger@physics.gatech.edu

Abdallah Ougazzaden − *School of Electrical and Computer Engineering, Georgia Institute of Technology, GT-Lorraine, 57070 Metz, France; Unité Mixte Internationale 2958, CNRS-Georgia Tech, 57070 Metz, France;* orcid.org/0000-0002-9959-5280; Email: abdallah.ougazzaden@georgiatech-metz.fr

Authors

James Gigliotti − *School of Physics and School of Materials Science and Engineering, Georgia Institute of Technology, Atlanta, Georgia 30332, United States*

Xin Li − *School of Electrical and Computer Engineering, Georgia Institute of Technology, GT-Lorraine, 57070 Metz, France; Unité Mixte Internationale 2958, CNRS-Georgia Tech, 57070 Metz, France*

Suresh Sundaram − *School of Electrical and Computer Engineering, Georgia Institute of Technology, GT-Lorraine, 57070 Metz, France; Unité Mixte Internationale 2958, CNRS-Georgia Tech, 57070 Metz, France*

Dogukan Deniz − *School of Physics, Georgia Institute of Technology, Atlanta, Georgia 30332, United States*

Vladimir Prudkovskiy − *Institut Néel, CNRS-Université Grenoble Alpes, 38042 Cedex 9 Grenoble, France; School of Physics, Georgia Institute of Technology, Atlanta, Georgia 30332, United States*

Jean-Philippe Turmaud − *School of Physics, Georgia Institute of Technology, Atlanta, Georgia 30332, United States*

Yiran Hu − *School of Physics, Georgia Institute of Technology, Atlanta, Georgia 30332, United States*

Yue Hu − *School of Physics, Georgia Institute of Technology, Atlanta, Georgia 30332, United States*

Frédéric Fossard − *Laboratoire d'Etude des Microstructures, ONERA-CNRS, Université Paris Saclay, F-92322 Châtillon, France;* orcid.org/0000-0002-7886-5309

Jean-Sébastien Mérot − *Laboratoire d'Etude des Microstructures, ONERA-CNRS, Université Paris Saclay, F-92322 Châtillon, France*

Annick Loiseau − *Laboratoire d'Etude des Microstructures, ONERA-CNRS, Université Paris Saclay, F-92322 Châtillon, France;* orcid.org/0000-0002-1042-5876

Gilles Patriarche − *Centre de Nanosciences et de Nanotechnologies, CNRS, Université Paris-Saclay, F-91460 Marcoussis, France*

Bokwon Yoon − *School of Physics, Georgia Institute of Technology, Atlanta, Georgia 30332, United States*

Uzi Landman − *School of Physics, Georgia Institute of Technology, Atlanta, Georgia 30332, United States*

Walt A. de Heer − *School of Physics, Georgia Institute of Technology, Atlanta, Georgia 30332, United States; Tianjin International Center of Nanoparticles and Nanosystems, Tianjin University, Tianjin 300072, China*

Complete contact information is available at: https://pubs.acs.org/10.1021/acsnano.0c04164

Notes

The authors declare no competing financial interest.

ACKNOWLEDGMENTS

Financial support was provided by the AFOSR under grant #FA9550-13-0217 and NSF #1506006. The work of U.L. and B.Y. was supported by the AFOSR grant #FA9550-15-1-0519. Calculations were carried out at the GATECH Center for Computational Materials Science. This work was also made possible by the French American Cultural Exchange council through a Partner University Fund project. C.B., V.P., F.F., and A.L. acknowledge funding from the European Union's Horizon 2020 research and innovation program under grant agreement No. 696656 (Graphene Core 1) and No. 785219 (Graphene Core 2).

REFERENCES

(1) Berger, C.; Song, Z. M.; Li, T. B.; Li, X. B.; Ogbazghi, A. Y.; Feng, R.; Dai, Z. T.; Marchenkov, A. N.; Conrad, E. H.; First, P. N.; De Heer, W. A. Ultrathin Epitaxial Graphite: 2D Electron Gas Properties and a Route toward Graphene-Based Nanoelectronics. *J. Phys. Chem. B* **2004**, *108*, 19912−19916.

(2) Berger, C.; Conrad, E.; de Heer, W. A. Epigraphene. In *Physics of Solid Surfaces, Landolt Börstein encyclopedia, New Series, Subvolume III/45B*; Chiarotti, G., Chiaradia, P., Eds.; Springer-Verlag: Berlin Heidelberg, Germany, 2018; pp 727−807.

(3) Das Sarma, S.; Adam, S.; Hwang, E. H.; Rossi, E. Electronic Transport in Two-Dimensional Graphene. *Rev. Mod. Phys.* **2011**, *83*, 407−466.

(4) Chen, J. H.; Jang, C.; Xiao, S. D.; Ishigami, M.; Fuhrer, M. S. Intrinsic and Extrinsic Performance Limits of Graphene Devices on SiO2. *Nat. Nanotechnol.* **2008**, *3*, 206−209.

(5) Dean, C. R.; Young, A. F.; Meric, I.; Lee, C.; Wang, L.; Sorgenfrei, S.; Watanabe, K.; Taniguchi, T.; Kim, P.; Shepard, K. L.; Hone, J. Boron Nitride Substrates for High-Quality Graphene Electronics. *Nat. Nanotechnol.* **2010**, *5*, 722−726.

(6) Kim, K. K.; Hsu, A.; Jia, X.; Kim, S. M.; Shi, Y.; Dresselhaus, M.; Palacios, T.; Kong, J. Synthesis and Characterization of Hexagonal Boron Nitride Film as a Dielectric Layer for Graphene Devices. *ACS Nano* **2012**, *6*, 8583−8590.

(7) Bresnehan, M. S.; Hollander, M. J.; Wetherington, M.; LaBella, M.; Trumbull, K. A.; Cavalero, R.; Snyder, D. W.; Robinson, J. A. Integration of Hexagonal Boron Nitride with Quasi-Freestanding Epitaxial Graphene: Toward Wafer-Scale, High-Performance Devices. *ACS Nano* **2012**, *6*, 5234−5241.
(8) Lee, K. H.; Shin, H.-J.; Lee, J.; Lee, I.-y.; Kim, G.-H.; Choi, J.-Y.; Kim, S.-W. Large-Scale Synthesis of High-Quality Hexagonal Boron Nitride Nanosheets for Large-Area Graphene Electronics. *Nano Lett.* **2012**, *12*, 714−718.
(9) Wang, M.; Jang, S. K.; Jang, W.-J.; Kim, M.; Park, S.-Y.; Kim, S.-W.; Kahng, S.-J.; Choi, J.-Y.; Ruoff, R. S.; Song, Y. J.; Lee, S. A Platform for Large-Scale Graphene Electronics − CVD Growth of Single-Layer Graphene on CVD-Grown Hexagonal Boron Nitride. *Adv. Mater.* **2013**, *25*, 2746−2752.
(10) Ponomarenko, L. A.; Gorbachev, R. V.; Yu, G. L.; Elias, D. C.; Jalil, R.; Patel, A. A.; Mishchenko, A.; Mayorov, A. S.; Woods, C. R.; Wallbank, J. R.; Mucha-Kruczynski, M.; Piot, B. A.; Potemski, M.; Grigorieva, I. V.; Novoselov, K. S.; Guinea, F.; Fal'ko, V. I.; Geim, A. K. Cloning of Dirac Fermions in Graphene Superlattices. *Nature* **2013**, *497*, 594−597.
(11) Purdie, D. G.; Pugno, N. M.; Taniguchi, T.; Watanabe, K.; Ferrari, A. C.; Lombardo, A. Cleaning Interfaces in Layered Materials Heterostructures. *Nat. Commun.* **2018**, *9*, 5387.
(12) Hemmi, A.; Bernard, C.; Cun, H.; Roth, S.; Klöckner, M.; Kälin, T.; Weinl, M.; Gsell, S.; Schreck, M.; Osterwalder, J.; Greber, T. High Quality Single Atomic Layer Deposition of Hexagonal Boron Nitride on Single Crystalline Rh(111) Four-Inch Wafers. *Rev. Sci. Instrum.* **2014**, *85*, No. 035101.
(13) Shi, Y. M.; Hamsen, C.; Jia, X. T.; Kim, K. K.; Reina, A.; Hofmann, M.; Hsu, A. L.; Zhang, K.; Li, H. N.; Juang, Z. Y.; Dresselhaus, M. S.; Li, L. J.; Kong, J. Synthesis of Few-Layer Hexagonal Boron Nitride Thin Film by Chemical Vapor Deposition. *Nano Lett.* **2010**, *10*, 4134−4139.
(14) Ismach, A.; Chou, H.; Ferrer, D. A.; Wu, Y.; McDonnell, S.; Floresca, H. C.; Covacevich, A.; Pope, C.; Piner, R.; Kim, M. J.; Wallace, R. M.; Colombo, L.; Ruoff, R. S. Toward the Controlled Synthesis of Hexagonal Boron Nitride Films. *ACS Nano* **2012**, *6*, 6378−6385.
(15) Roth, S.; Matsui, F.; Greber, T.; Osterwalder, J. Chemical Vapor Deposition and Characterization of Aligned and Incommensurate Graphene/Hexagonal Boron Nitride Heterostack on Cu(111). *Nano Lett.* **2013**, *13*, 2668−2675.
(16) Jin, W.; Yeh, P.-C.; Zaki, N.; Chenet, D.; Arefe, G.; Hao, Y.; Sala, A.; Mentes, T. O.; Dadap, J. I.; Locatelli, A.; Hone, J.; Osgood, R. M. Tuning the Electronic Structure of Monolayer Graphene/MoS_2 van der Waals Heterostructures *via* Interlayer Twist. *Phys. Rev. B: Condens. Matter Mater. Phys.* **2015**, *92*, 201409.
(17) Ge, S.; Habib, K. M. M.; De, A.; Barlas, Y.; Wickramaratne, D.; Neupane, M. R.; Lake, R. K. Interlayer Transport through a Graphene/Rotated Boron Nitride/Graphene Heterostructure. *Phys. Rev. B: Condens. Matter Mater. Phys.* **2017**, *95*, No. 045303.
(18) Wang, D.; Chen, G.; Li, C.; Cheng, M.; Yang, W.; Wu, S.; Xie, G.; Zhang, J.; Zhao, J.; Lu, X.; Chen, P.; Wang, G.; Meng, J.; Tang, J.; Yang, R.; He, C.; Liu, D.; Shi, D.; Watanabe, K.; Taniguchi, T.; Feng, J.; Zhang, Y.; Zhang, G. Thermally Induced Graphene Rotation on Hexagonal Boron Nitride. *Phys. Rev. Lett.* **2016**, *116*, 126101.
(19) Liu, Z.; Song, L.; Zhao, S. Z.; Huang, J. Q.; Ma, L. L.; Zhang, J. N.; Lou, J.; Ajayan, P. M. Direct Growth of Graphene/Hexagonal Boron Nitride Stacked Layers. *Nano Lett.* **2011**, *11*, 2032−2037.
(20) Alaboson, J. M. P.; Wang, Q. H.; Emery, J. D.; Lipson, A. L.; Bedzyk, M. J.; Elam, J. W.; Pellin, M. J.; Hersam, M. C. Seeding Atomic Layer Deposition of High-k Dielectrics on Epitaxial Graphene with Organic Self-Assembled Monolayers. *ACS Nano* **2011**, *5*, 5223−5232.
(21) Song, Y. X.; Zhang, C. R.; Li, B.; Ding, G. Q.; Jiang, D.; Wang, H. M.; Xie, X. M. Van der Waals Epitaxy and Characterization of Hexagonal Boron Nitride Nanosheets on Graphene. *Nanoscale Res. Lett.* **2014**, *9*, 367.
(22) Sediri, H.; Pierucci, D.; Hajlaoui, M.; Henck, H.; Patriarche, G.; Dappe, Y. J.; Yuan, S.; Toury, B.; Belkhou, R.; Silly, M. G.; Sirotti, F.; Boutchich, M.; Ouerghi, A. Atomically Sharp Interface in an h-BN-Epitaxial Graphene van der Waals Heterostructure. *Sci. Rep.* **2015**, *5*, 16465.
(23) Gopalan, D. P.; Mende, P. C.; de la Barrera, S. C.; Dhingra, S.; Li, J.; Zhang, K.; Simonson, N. A.; Robinson, J. A.; Lu, N.; Wang, Q.; Kim, M. J.; D'Urso, B.; Feenstra, R. M. Formation of Hexagonal Boron Nitride on Graphene-Covered Copper Surfaces. *J. Mater. Res.* **2016**, *31*, 945−958.
(24) Cheng, T. S.; Summerfield, A.; Mellor, C. J.; Davies, A.; Khlobystov, A. N.; Eaves, L.; Foxon, C. T.; Beton, P. H.; Novikov, S. V. High-Temperature Molecular Beam Epitaxy of Hexagonal Boron Nitride Layers. *J. Vac. Sci. Technol., B: Nanotechnol. Microelectron.: Mater., Process., Meas., Phenom.* **2018**, *36*, No. 02D103.
(25) Pierucci, D.; Zribi, J.; Henck, H.; Chaste, J.; Silly, M. G.; Bertran, F.; Le Fevre, P.; Gil, B.; Summerfield, A.; Beton, P. H.; Novikov, S. V.; Cassabois, G.; Rault, J. E.; Ouerghi, A. van der Waals Epitaxy of Two-Dimensional Single-Layer h-BN on Graphite by Molecular Beam Epitaxy: Electronic Properties and Band Structure. *Appl. Phys. Lett.* **2018**, *112*, 253102.
(26) Elias, C.; Valvin, P.; Pelini, T.; Summerfield, A.; Mellor, C. J.; Cheng, T. S.; Eaves, L.; Foxon, C. T.; Beton, P. H.; Novikov, S. V.; Gil, B.; Cassabois, G. Direct Band-Gap Crossover in Epitaxial Monolayer Boron Nitride. *Nat. Commun.* **2019**, *10*, 2639.
(27) Miwa, J. A.; Dendzik, M.; Grønborg, S. S.; Bianchi, M.; Lauritsen, J. V.; Hofmann, P.; Ulstrup, S. van der Waals Epitaxy of Two-Dimensional MoS2−Graphene Heterostructures in Ultrahigh Vacuum. *ACS Nano* **2015**, *9*, 6502−6510.
(28) Koos, A. A.; Vancsó, P.; Magda, G. Z.; Osváth, Z.; Kertész, K.; Dobrik, G.; Hwang, C.; Tapasztó, L.; Biró, L. P. STM Study of the MoS2 Flakes Grown on Graphite: A model System for Atomically Clean 2D Heterostructure Interfaces. *Carbon* **2016**, *105*, 408−415.
(29) Bianco, G. V.; Losurdo, M.; Giangregorio, M. M.; Sacchetti, A.; Prete, P.; Lovergine, N.; Capezzuto, P.; Bruno, G. Direct Epitaxial CVD Synthesis of Tungsten Disulfide on Epitaxial and CVD Graphene. *RSC Adv.* **2015**, *5*, 98700−98708.
(30) Huang, J.-K.; Pu, J.; Hsu, C.-L.; Chiu, M.-H.; Juang, Z.-Y.; Chang, Y.-H.; Chang, W.-H.; Iwasa, Y.; Takenobu, T.; Li, L.-J. Large-Area Synthesis of Highly Crystalline WSe2Monolayers and Device Applications. *ACS Nano* **2014**, *8*, 923−930.
(31) Eichfeld, S. M.; Hossain, L.; Lin, Y.-C.; Piasecki, A. F.; Kupp, B.; Birdwell, A. G.; Burke, R. A.; Lu, N.; Peng, X.; Li, J.; Azcatl, A.; McDonnell, S.; Wallace, R. M.; Kim, M. J.; Mayer, T. S.; Redwing, J. M.; Robinson, J. A. Highly Scalable, Atomically Thin WSe2 Grown *via* Metal−Organic Chemical Vapor Deposition. *ACS Nano* **2015**, *9*, 2080−2087.
(32) Chubarov, M.; Pedersen, H.; Högberg, H.; Jensen, J.; Henry, A. Growth of High Quality Epitaxial Rhombohedral Boron Nitride. *Cryst. Growth Des.* **2012**, *12*, 3215−3220.
(33) Li, X.; Sundaram, S.; El Gmili, Y.; Ayari, T.; Puybaret, R.; Patriarche, G.; Voss, P. L.; Salvestrini, J. P.; Ougazzaden, A. Large-Area Two-Dimensional Layered Hexagonal Boron Nitride Grown on Sapphire by Metalorganic Vapor Phase Epitaxy. *Cryst. Growth Des.* **2016**, *16*, 3409−3415.
(34) Majety, S.; Li, J.; Zhao, W. P.; Huang, B.; Wei, S. H.; Lin, J. Y.; Jiang, H. X. Hexagonal Boron Nitride and 6H-SiC Heterostructures. *Appl. Phys. Lett.* **2013**, *102*, 213505.
(35) Snure, M.; Paduano, Q.; Kiefer, A. Effect of Surface Nitridation On the Epitaxial Growth of Few-Layer sp2 BN. *J. Cryst. Growth* **2016**, *436*, 16−22.
(36) Schue, L.; Stenger, I.; Fossard, F.; Loiseau, A.; Barjon, J. Characterization Methods Dedicated to Nanometer-Thick hBN Layers. *2D Mater.* **2017**, *4*, No. 015028.
(37) Jang, A. R.; Hong, S.; Hyun, C.; Yoon, S. I.; Kim, G.; Jeong, H. Y.; Shin, T. J.; Park, S. O.; Wong, K.; Kwak, S. K.; Park, N.; Yu, K.; Choi, E.; Mishchenko, A.; Withers, F.; Novoselov, K. S.; Lim, H.; Shin, H. S. Wafer-Scale and Wrinkle-Free Epitaxial Growth of Single-

https://dx.doi.org/10.1021/acsnano.0c04164
ACS Nano 2020, 14, 12962−12971

Orientated Multilayer Hexagonal Boron Nitride on Sapphire. *Nano Lett.* **2016**, *16*, 3360−3366.
(38) Emery, J. D.; Wheeler, V. H.; Johns, J. E.; McBriarty, M. E.; Detlefs, B.; Hersam, M. C.; Gaskill, D. K.; Bedzyk, M. J. Structural Consequences of Hydrogen intercalation of Epitaxial Graphene on SiC(0001). *Appl. Phys. Lett.* **2014**, *105*, 161602.
(39) Riedl, C.; Coletti, C.; Iwasaki, T.; Zakharov, A. A.; Starke, U. Quasi-Free-Standing Epitaxial Graphene on SiC Obtained by Hydrogen Intercalation. *Phys. Rev. Lett.* **2009**, *103*, 246804.
(40) Sutter, P.; Cortes, R.; Lahiri, J.; Sutter, E. Interface Formation in Monolayer Graphene-Boron Nitride Heterostructures. *Nano Lett.* **2012**, *12*, 4869−4874.
(41) Geng, D.; Dong, J.; Kee Ang, L.; Ding, F.; Yang, H. Y. *In Situ* Epitaxial Engineering of Graphene and h-BN Lateral Heterostructure With a Tunable Morphology Comprising h-BN Domains. *NPG Asia Mater.* **2019**, *11*, 56.
(42) Stehle, Y.; Meyer, H. M.; Unocic, R. R.; Kidder, M.; Polizos, G.; Datskos, P. G.; Jackson, R.; Smirnov, S. N.; Vlassiouk, I. V. Synthesis of Hexagonal Boron Nitride Monolayer: Control of Nucleation and Crystal Morphology. *Chem. Mater.* **2015**, *27*, 8041−8047.
(43) Shinde, S. M.; Dhakal, K. P.; Chen, X.; Yun, W. S.; Lee, J.; Kim, H.; Ahn, J.-H. Stacking-Controllable Interlayer Coupling and Symmetric Configuration of Multilayered MoS2. *NPG Asia Mater.* **2018**, *10*, e468.
(44) Chen, J. J.; Zhu, E. B.; Liu, J.; Zhang, S.; Lin, Z. Y.; Duan, X. F.; Heinz, H.; Huang, Y.; De Yoreo, J. J. Building Two-Dimensional Materials One Row at a Time: Avoiding The Nucleation Barrier. *Science* **2018**, *362*, 1135.
(45) Kashchiev, D. *Nucleation: Basic Theory with Applications*; Butterworth-Heinemann, 2000.
(46) Yang, W.; Chen, G. R.; Shi, Z. W.; Liu, C. C.; Zhang, L. C.; Xie, G. B.; Cheng, M.; Wang, D. M.; Yang, R.; Shi, D. X.; Watanabe, K.; Taniguchi, T.; Yao, Y. G.; Zhang, Y. B.; Zhang, G. Y. Epitaxial Growth of Single-Domain Graphene on Hexagonal Boron Nitride. *Nat. Mater.* **2013**, *12*, 792−797.
(47) de Heer, W. A.; Berger, C.; Ruan, M.; Sprinkle, M.; Li, X.; Hu, Y.; Zhang, B.; Hankinson, J.; Conrad, E. H. Large Area and Structured Epitaxial Graphene Produced by Confinement Controlled Sublimation of Silicon Carbide. *Proc. Natl. Acad. Sci. U. S. A.* **2011**, *108*, 16900−16905.
(48) Berger, C.; Deniz, D.; Gigliotti, J.; Palmer, J.; Hankinson, J.; Hu, Y.; Turmaud, J.-P.; Puybaret, R.; Ougazzaden, A.; Sidorov, A.; Jiang, Z.; de Heer, W. A. Epitaxial Graphene on SiC: 2D Sheets, Selective Growth and Nanoribbons. In *Growing Graphene on Semiconductors*; Motta, N., Coletti, C., Iacopi, F., Eds.; PanStanford: Singapore, 2017; p 181.
(49) Li, X.; Sundaram, S.; Gmili, Y. E.; Moudakir, T.; Genty, F.; Bouchoule, S.; Patriarche, G.; Dupuis, R. D.; Voss, P. L.; Salvestrini, J.-P.; Ougazzaden, A. BAlN Thin Layers For Deep UV Applications. *Phys. Status Solidi A* **2015**, *212*, 745−750.
(50) Kresse, G.; Joubert, D. From Ultrasoft Pseudopotentials to the Projector Augmented-Wave Method. *Phys. Rev. B: Condens. Matter Mater. Phys.* **1999**, *59*, 1758−1775.
(51) Perdew, J. P.; Burke, K.; Ernzerhof, M. Generalized Gradient Approximation Made Simple. *Phys. Rev. Lett.* **1996**, *77*, 3865−3868.

https://dx.doi.org/10.1021/acsnano.0c04164
ACS Nano 2020, 14, 12962−12971